Spontaneous Formation of a Superconductor–Topological Insulator–Normal Metal Layered Heterostructure

Yu-Qi Wang, Xu Wu, Ye-Liang Wang, Yan Shao, Tao Lei, Jia-Ou Wang, Shi-Yu Zhu, Haiming Guo, Ling-Xiao Zhao, Gen-Fu Chen, Simin Nie, Hong-Ming Weng, Kurash Ibrahim, Xi Dai, Zhong Fang, and Hong-Jun Gao**

The discovery of graphene has spurred vigorous investigation of 2D materials, revealing a wide range of extraordinary properties and functionalities. 2D heterostructural materials have recently been fabricated by assembling isolated planes layer-by-layer in a desired sequence. Unusual properties and novel physical phenomena have been unveiled in such layered heterostructures.[1–4] For example, Hofstadter's butterfly, an intriguing pattern of the energy states of Bloch electrons, was predicted several decades ago to be observable only under unfeasibly strong magnetic fields in conventional materials. But it has been observed recently under current experimental conditions in graphene/BN layered heterostructures, one of the outstanding new kinds of 2D materials.[5–8] Moreover, another amazing physics phenomenon, Majorana fermions was predicted to exist in heterostructural systems consisting of a superconductor (SC) and a topological insulator (TI).[9–14] The coupling between an s-wave superconductor and the edge state of a 2D topological insulator can produce the long-sought Majorana quasiparticle excitations, with outstanding applications for high-efficiency quantum computation in the future.[9–22] The key to observing the Majorana phenomenon experimentally is finding ideal material systems, typically by construction of TI/SC hybrid structures. A few such heterostructures have been reported, fabricated by stacking different low-dimensional materials.[19–22] However, the transfer and stacking process involves complicated steps of advanced microfabrication techniques. Certainly, it is essential both to explore more related heterostructures and to develop new approaches, like a method based on spontaneous formation of desired heterostructures, for both fundamental research and technological applications.

In particular, we note that $HfTe_5$ films in few-layer thickness have recently been theoretically predicted as a promising large-gap topological insulator.[23] $HfTe_3$ bulk has been reported as a superconductivity experimentally.[24] Interestingly, these two materials have a layered configuration in the *a-c* plane. In the *a-c* plane, a $HfTe_5$ layer can be considered as a $HfTe_3$ layer linked via Te—Te chains (see models in **Figure 1**d,e; Figure S1 in the Supporting Information).[23,25–27] In addition, an idea for a spontaneous structural transformation from $HfTe_5$ to $HfTe_3$ can be spurred by analyzing the Hf-Te binary phase diagram, which showing these two structures are neighboring phases and the phase transition is possible under proper temperature. All these data from literatures provide hint for the formation of a $HfTe_3/HfTe_5$ heterostructure with combined properties of topological insulator and superconductor. Besides the bulk materials, however, either $HfTe_3$ or $HfTe_5$ films are not reported experimentally yet. This stimulates us to explore a spontaneous way to construct such film materials and their layered heterostructures. This method may lay the groundwork for the construction of novel 2D systems with integrated properties in few-layer thickness, suitable for superconducting devices and experimental realization of Majorana fermions.

Here we report fabricating a superconductor–topological insulator–normal metal heterostructure with a layered configuration of $HfTe_3/HfTe_5/Hf$ for the first time. By optimizing the experimental process, we find that this heterostructure can indeed form spontaneously. The atomic structure of the heterostructure has been determined by in situ scanning tunneling microscopy (STM) and X-ray photoelectron spectroscopy (XPS). Scanning tunneling spectroscopy (STS) measurements directly reveal a bandgap as large as 60 meV in $HfTe_5$ film and a superconducting spectrum in $HfTe_3/HfTe_5$ film. Such a heterostructure is potentially suitable for studying many amazing phenomena including Majorana bound states.[9–14] Unlike the artificial film lift-transfer-stacking technique, our current method of making desired heterostructures is based on a spontaneous formation process of surface reaction and epitaxial growth and significantly simplifies the fabrication process. This method may offer new routes for the development of other related functional heterostructures and nanodevices.

The $HfTe_3/HfTe_5$ heterostructures were fabricated through direct reaction and epitaxial growth of tellurium atoms on a Hf(0001) substrate (see the schematic in Figure 1). Our method

Y.-Q. Wang, X. Wu, Prof. Y.-L. Wang, Y. Shao, Dr. J.-O. Wang, S.-Y. Zhu, Dr. H. Guo, L.-X. Zhao, Prof. G.-F. Chen, S. Nie, Dr. H.-M. Weng, Prof. X. Dai, Prof. Z. Fang, Prof. H.-J. Gao
Beijing National Laboratory of Condensed Matter Physics
Institute of Physics
Chinese Academy of Sciences
Beijing 100190, P. R. China
E-mail: ylwang@iphy.ac.cn; hjgao@iphy.ac.cn
Y.-Q. Wang, T. Lei, Prof. K. Ibrahim
Institute of High Energy Physics
Chinese Academy of Sciences
Beijing 100049, P. R. China
Prof. Y.-L. Wang, Prof. G.-F. Chen, Dr. H.-M. Weng, Prof. X. Dai, Prof. Z. Fang, Prof. H.-J. Gao
Collaborative Innovation Center of Quantum Matter
Beijing 100084, P. R. China

DOI: 10.1002/adma.201600575

ADVANCED MATERIALS
www.advmat.de

Materials Views
www.MaterialsViews.com

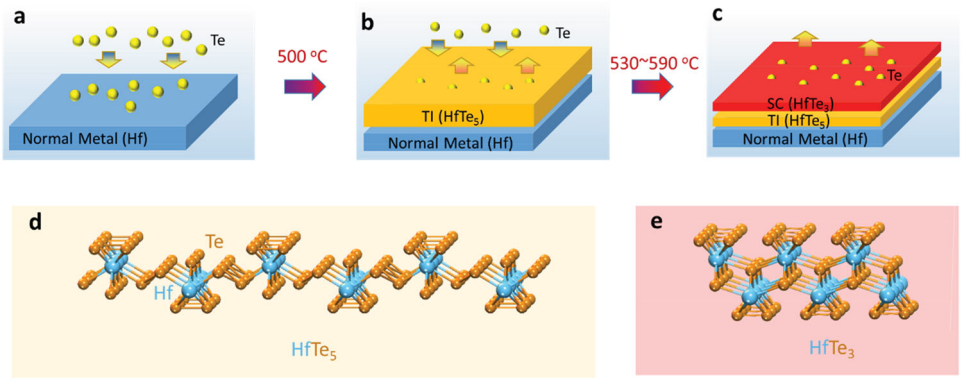

Figure 1. Schematic of the fabrication process. A superconductor–topological insulator–normal metal heterostructure is constructed by a single step of direct reaction and epitaxial growth of tellurium atoms on a Hf(0001) substrate. a) Tellurium atoms are deposited on Hf(0001) substrate at room temperature. b) The substrate is then annealed to 500 °C during deposition of Te atoms, and epitaxial insulated $HfTe_5$ film (indicated in yellow) is obtained. c) While the substrate is further annealed to 530–590 °C without deposition of Te atoms, the topmost layer of the $HfTe_5$ film transforms into superconductive $HfTe_3$ film (indicated in red) due to some of the Te atoms escaping from the $HfTe_5$ film. As a result, a $HfTe_3/HfTe_5$/Hf layered heterostructure is obtained. d,e) 3D view of $HfTe_5$ and $HfTe_3$ single-layer structure, respectively.

for forming this heterostructure is a straightforward and transfer-free technique. Only tellurium atoms were deposited on a Hf(0001) substrate (Figure 1a). The substrate was annealed to 500 °C while depositing Te atoms to obtain epitaxial $HfTe_5$ film (Figure 1b). Then the substrate was annealed to 530–590 °C without depositing Te atoms to obtain epitaxial $HfTe_3$ film at the top of the sample (Figure 1c).

To investigate the atomic structure of the as-grown epitaxial films described in Figure 1b, we performed STM studies. **Figure 2**a is a large-scale STM image of the sample. The zoom-in image (Figure 2b) shows a well-ordered pattern of protrusions with rectangular symmetry and crystalline constant of the *a*-*c* plane in $HfTe_5$ bulk material (more discussions are presented in Figure S1 in the Supporting Information).[23,25,26] Moreover, the formation of $HfTe_5$ film was monitored by in situ X-ray photoemission spectroscopy (XPS). The XPS data from this $HfTe_5$ film were consistent with those of $HfTe_5$ single crystal (see Figure S2 in the Supporting Information). With a combination of these data, we conclude that a $HfTe_5$ film is formed on the substrate at this stage. In Figure 2b, the surfaces show certain amount of defects, which are probably due to the lack of Te atoms at related high sample annealing temperature.

In order to further reveal the electronic properties of the $HfTe_5$ film, we performed STS measurements (Figure 2c). STS detects the differential tunneling conductance (dI/dV), which gives a measure of the local density of states of the samples near the Fermi level (zero bias) of electrons at energy eV. The dI/dV spectra in Figure 2c show that the Fermi level is within

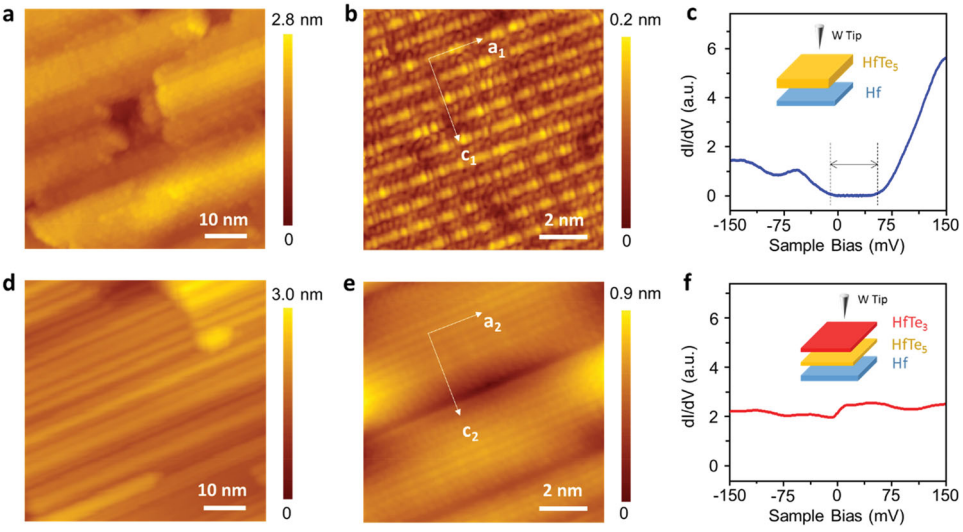

Figure 2. Structural and electronic properties of the as-grown films, obtained by STM/STS. a) STM topographic image (–1.00 V, –1.00 pA) of the $HfTe_5$ film. b) High-resolution image (50.0 mV, 1.00 nA) of the $HfTe_5$ film. c) dI/dV spectrum (setpoint, –200 mV, –100 pA) taken at $HfTe_5$ surface. The black arrow and the dashed lines indicate the bottom of the conduction band (right) and the top of the valence band (left), respectively. d) Topographic image (–5.00 V, –10.0 pA) of the $HfTe_3$ film. e) High-resolution image (–200 mV, –500 pA) of the $HfTe_3$ film. f) dI/dV spectrum (setpoint, –300 mV, –100 pA) taken at $HfTe_3$ surface. The arrows in (b) and (e) indicate the close-packed symmetric crystalline directions in the *a*–*c* plane. Insets in (c) and (f) show schematics of a tungsten tip located at the surface of the $HfTe_5$/Hf and a $HfTe_3/HfTe_5$/Hf heterostructure, respectively.

the energy gap. This energy gap is as large as 60 meV, and is close to the energy gap theoretically calculated for $HfTe_5$ with a thickness of three layers (see Figure S3 in the Supporting Information), providing further clear evidence of the formation of $HfTe_5$ film. This film is identified as a topological insulator in theoretical prediction.[23,28]

We then conducted further thermal treatment of the sample with increasing sample temperatures to drive the formation of $HfTe_3$ film at the top of the substrate, as described in Figure 1c. Figure 2d is a large-scale STM image of the treated sample. We can see that its topography is clearly different from that of $HfTe_5$ film shown in Figure 2a. Figure 2e is a zoom-in image of the annealed sample. The well-ordered protrusions in this image exhibit a rectangular lattice (the model is shown in Figure S1 in the Supporting Information). The periodicities of these protrusions match the crystalline constants in the *a*-*c* plane in $HfTe_3$ bulk.[29] The electronic properties of $HfTe_3$ film were also investigated by STS at sample temperature of 4 K, as shown by the dI/dV spectrum in Figure 2f, the feature in which is obviously different from that of $HfTe_5$ film (Figure 2c). One significant difference is that no bandgap exists in the $HfTe_3$ film, while $HfTe_5$ film has an energy bandgap of 60 meV. The Hf–Te interaction in an individual $HfTe_5$ or $HfTe_3$ layer is quite stronger than the van der Waals interaction among the layers. The transition from $HfTe_5$ to $HfTe_3$ should happen in an individual layer and result in an epitaxial interface.

To confirm and analyze the possible superconducting properties of the resulting $HfTe_3$ film, dI/dV spectra were further obtained at various sample temperatures and externally applied magnetic fields, which are often utilized together to determine a material's superconductivity. In the as-prepared $HfTe_3$ film, we indeed observed superconducting gap-like spectra: a pronounced dip in the density of states at the Fermi level, and one peak existing on each side of this dip (see dI/dV spectra in Figure 3a,c; Figure S4, Supporting Information). **Figure 3**a shows the spectra measured at different sample temperatures from 0.48 to 0.93 K with interval of 0.1 K. From these experimental spectra, the superconducting gap (Δ), critical temperature (T_C) for superconductor and the Bardeen–Cooper–Schrieffer (BCS) ratio $2\Delta/k_BT_C$ (k_B is the Boltzmann constant) can be deduced by the BCS fitting,[30] the values are 0.20 meV, 1.23 K, and 3.75, respectively (Figure 3b). The superconducting property of $HfTe_3$ film is further supported by STS experiments under variable external magnetic fields. Figure 3c shows the dI/dV spectra obtained at magnetic fields from 0 to 6 T, applied to the sample surface in vertical direction. By a systematic analysis of the zero-bias conductance (ZBC) in these field-dependent dI/dV spectra, an upper critical field (H_{C2}) of 5.76 T for completely suppressing superconductivity can be obtained (Figure 3d). Thus, these combined measurements verified the superconducting properties of the $HfTe_3$ film.

To gain further insight into the epitaxial film and its growth process, we performed in situ XPS studies of the formation process of the heterostructure. **Figure 4**a shows the XPS spectra of the Te_{3d} core level during the growth of the film with increasing sample temperatures. After the substrate was annealed to ≈500 °C while depositing Te atoms, two peaks of binding energy (marked in red at binding energies 582.82 and 572.42 eV) are the same as those of $HfTe_5$ single crystal (Figure S5 in Supporting Information). These two peaks can be assigned to the $HfTe_5$ film, as revealed by the STM measurements at this stage (Figure 2a). Further increasing the sample temperature up to 530 °C without depositing Te atoms, as described in Figure 1c, results in decreased intensity of the red peaks (at 582.82 and 572.42 eV), while two new peaks appear (marked by the purple at binding energies 583.47 and 573.0 eV). These two purple peaks can be assigned to the $HfTe_3$ film, as analyzed by the STM measurements (Figure 2d). Even at ≈590 °C, the intensity of purple peaks increases while the red peaks still exist, demonstrating the coexistence of $HfTe_5$ and $HfTe_3$ films.

Another issue is the stacking order of the $HfTe_3$ and $HfTe_5$ films. We found that the geometric structure of the whole sample surface is the same as the STM observation in Figure 2d, indicating that the topmost layer of the sample is $HfTe_3$ film. We also found that different samples prepared

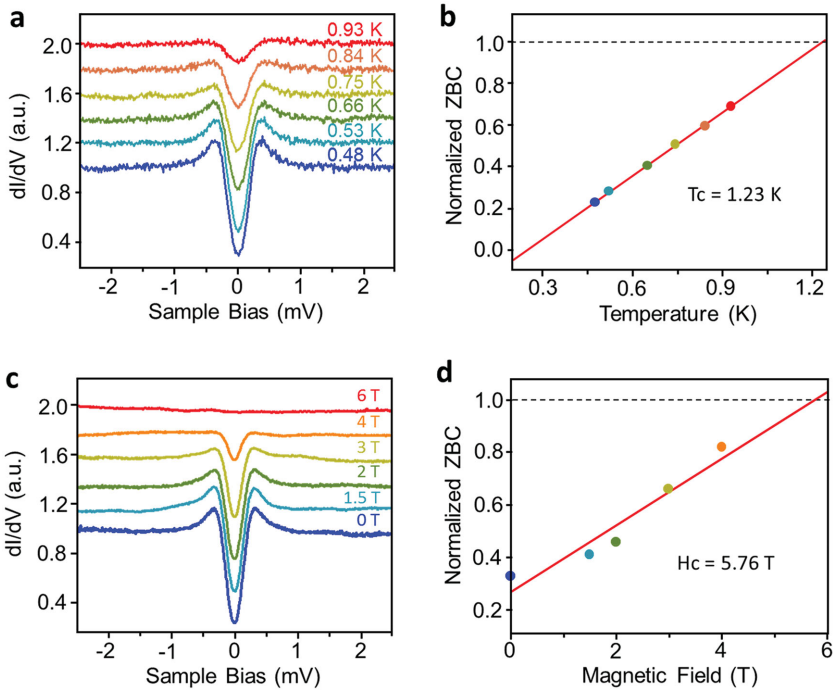

Figure 3. Superconductivity on the as-grown $HfTe_3$ film. a) Differential conductance measured with a W tip on the $HfTe_3$ film as a function of sample temperatures. The curves at different temperatures are offset vertically for clarity. b) The open circles show the measured gap and the solid curve shows the fitting by the BCS gap function. c) The differential conductance measured on the $HfTe_3$ film as a function of external magnetic field. The tunneling junction (also applies to (a)) was set at $V = 40$ mV and $I = 200$ pA. d) The dots show the normalized ZBC from the spectra in (c). The upper critical field of the $HfTe_3$ film for completely suppressing superconductivity is estimated to be 5.76 T.

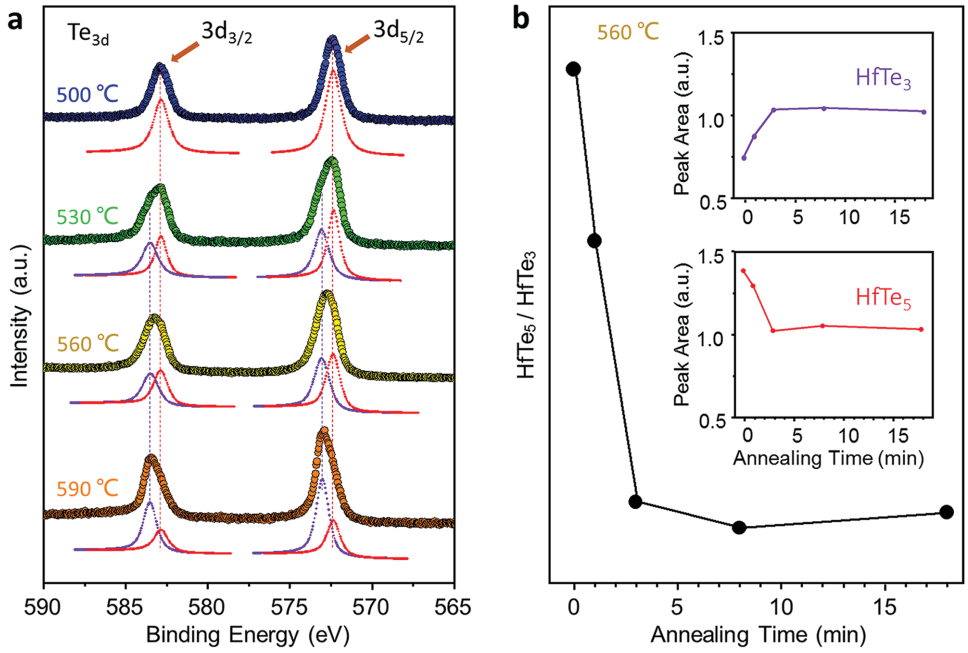

Figure 4. XPS measurements during the evolution of the heterostructure. a) The binding energies of Te_{3d} as a function of the sample temperature. The red peak positions (582.82 and 572.42 eV) correspond to the binding energy of Te_{3d} in $HfTe_5$. The purple peak positions (583.47 and 573.0 eV) correspond to the binding energy of Te_{3d} in $HfTe_3$. b) Area ratio of Te_{3d} in $HfTe_5$ to Te_{3d} in $HfTe_3$ as a function of annealing time (the sample temperature was kept at 560 °C. Insets show the normalized peak area of Te_{3d} in $HfTe_5$ (red dots and line) and $HfTe_3$ (purple dots and line), respectively.

in same experimental conditions showed an identical geometric structure. To clarify the coexistence and layer order of the $HfTe_3/HfTe_5$ films, the ratios of photoemission peak area of Te_{3d} in $HfTe_5$ to Te_{3d} in $HfTe_3$ are measured as a function of annealing time (Figure 4b; Figure S5, Supporting Information). As shown by curves in the inset of Figure 4b, the peak area of Te_{3d} in $HfTe_3$ increases, while that in $HfTe_5$ decreases during the initial annealing stage. After an annealing time up to ≈3 min, both the peak areas of Te in $HfTe_3$ and in $HfTe_5$ remain constant. We therefore conclude that there is a $HfTe_5$ film between $HfTe_3$ film and the substrate. So a combined analysis of XPS, STM, and STS data demonstrates that a $HfTe_3/HfTe_5$ layered films is formed on the Hf substrate.

In summary, we successfully fabricated a heretofore-unexplored superconductor–topological insulator–normal metal heterostructure with a $HfTe_3/HfTe_5$/Hf layered configuration through direct reaction and epitaxial growth of Te atoms on a Hf(0001) substrate. The geometric structures and electrical properties of the heterostructure were experimentally determined by XPS, STM, and STS. This layered heterostructure has potential for studies of both the QSH effect and topological phase transitions.[23] Our newly demonstrated method opens up a route to fabricate heterostructures and nanodevices with a combination of multiproperties, particularly to form systems to study Majorana quasiparticle excitations and topological quantum computation.[31,32]

Experimental Section

Sample Preparation: The superconductor–topological insulator–normal metal $HfTe_3/HfTe_5$/Hf heterostructures were fabricated in an ultrahigh vacuum chamber, with a base pressure of 2×10^{-10} mbar, equipped with standard molecular beam epitaxy (MBE) capabilities. The Hf(0001) substrate was cleaned by several cycles of Ar^+ ion sputtering, followed by annealing until clean surface terraces were obtained in the STM images. Plenty of Te (Sigma, 99.999%) evaporated from a Knudsen cell was deposited onto the clean Hf(0001) surface at room temperature. The sample was subsequently annealed at proper temperatures to achieve different structures (at 500 °C for the $HfTe_5$ structure, and at about 560 °C for $HfTe_3/HfTe_5$ layered structures). After growth, the samples were transferred to STM equipment and cooled for imaging of topographies and measuring of the local electronic properties.

XPS Measurements: The in situ X-ray photoelectron spectroscopy measurements were performed at the Beijing Synchrotron Radiation Facility (BSRF). Synchrotron radiation light monochromated by four high-resolution gratings and controlled by a hemispherical energy analyzer has photon energy in the range from 10 to 1100 eV.

STM Measurements: To obtain the electronic structures of the films, STM experiments were performed using an ultralow-temperature STM system (Unisoku and RHK) operated at a base temperature of 0.45 K and under a magnetic field up to 9 T. The differential conductance (dI/dV) was measured using lock-in detection of the tunnel current I by adding a 5 mV for 4 K and 0.15 mV for 0.45 K modulated bias voltage at 973 Hz to the sample bias voltage V. The energy resolution is better than 0.4 meV at 0.45 K with an electrochemically etched tungsten tip.

Supporting Information

Supporting Information is available from the Wiley Online Library or from the author.

Acknowledgements

Y.Q.W. and X.W. contributed equally to this work. The authors acknowledge financial support from the National Basic Research Program of China (Grant Nos. 2013CBA01600 and 2015CB921103), National Natural Science Foundation of China (Grant Nos. 61222112,

51572290, 51325204, and 11334006), and Chinese Academy of Sciences (Grant Nos. 1731300500015 and XDB07030100).

Received: January 30, 2016
Revised: February 27, 2016
Published online: April 18, 2016

[1] A. K. Geim, I. V. Grigorieva, *Nature* **2013**, *499*, 419.
[2] L. Wang, B. Wu, J. Chen, H. Liu, P. Hu, Y. Liu, *Adv. Mater.* **2014**, *26*, 1559.
[3] X. Huang, C. Tan, Z. Yin, H. Zhang, *Adv. Mater.* **2014**, *26*, 2185.
[4] P. T. Loan, W. Zhang, C. T. Lin, K. H. Wei, L. J. Li, C. H. Chen, *Adv. Mater.* **2014**, *26*, 4838.
[5] B. Hunt, J. D. Sanchez-Yamagishi, A. F. Young, M. Yankowitz, *Science* **2013**, *340*, 1427.
[6] C. R. Dean, L. Wang, P. Maher, C. Forsythe, F. Ghahari, Y. Gao, J. Katoch, M. Ishigami, P. Moon, M. Koshino, T. Taniguchi, K. Watanabe, K. L. Shepard, J. Hone, P. Kim, *Nature* **2013**, *497*, 598.
[7] L. A. Ponomarenko, R. V. Gorbachev, G. L. Yu, D. C. Elias, R. Jalil, A. A. Patel, A. Mishchenko, A. S. Mayorov, C. R. Woods, J. R. Wallbank, M. Mucha-Kruczynski, B. A. Piot, M. Potemski, I. V. Grigorieva, K. S. Novoselov, F. Guinea, V. I. Fal'ko, A. K. Geim, *Nature* **2013**, *497*, 594.
[8] W. Yang, G. Chen, Z. Shi, C. C. Liu, L. Zhang, G. Xie, M. Cheng, D. Wang, R. Yang, D. Shi, K. Watanabe, T. Taniguchi, Y. Yao, Y. Zhang, G. Zhang, *Nat. Mater.* **2013**, *12*, 792.
[9] L. Fu, C. L. Kane, *Phys. Rev. Lett.* **2008**, *100*, 096407.
[10] F. Wilczek, *Nat. Phys.* **2009**, *5*, 614.
[11] M. Z. Hasan, C. L. Kane, *Rev. Mod. Phys.* **2010**, *82*, 3045.
[12] X.-L. Qi, S.-C. Zhang, *Rev. Mod. Phys.* **2011**, *83*, 1057.
[13] P. W. Brouwer, *Science* **2012**, *336*, 989.
[14] C. W. Beenakker, *J. Annu. Rev. Condens. Matter Phys.* **2013**, *4*, 113.
[15] J. Nilsson, A. R. Akhmerov, C. W. Beenakker, *J. Phys. Rev. Lett.* **2008**, *101*, 120403.
[16] R. M. Lutchyn, J. D. Sau, S. Das Sarma, *Phys. Rev. Lett.* **2010**, *105*, 077001.
[17] Y. Oreg, G. Refael, F. von Oppen, *Phys. Rev. Lett.* **2010**, *105*, 177002.
[18] V. Mourik, K. Zuo, S. M. Frolov, S. R. Plissard, E. Bakkers, L. P. Kouwenhoven, *Science* **2012**, *336*, 1003.
[19] A. Das, Y. Ronen, Y. Most, Y. Oreg, M. Heiblum, H. Shtrikman, *Nat. Phys.* **2012**, *8*, 887.
[20] M. T. Deng, C. L. Yu, G. Y. Huang, M. Larsson, P. H. Caroff, Q. Xu, *Nano Lett.* **2012**, *12*, 6414.
[21] A. D. Finck, D. J. Van Harlingen, P. K. Mohseni, K. Jung, X. Li, *Phys. Rev. Lett.* **2013**, *110*, 126406.
[22] N.-S. Perge, I. K. Drozdov, J. Li, H. Chen, S. Jeon, J. Seo, A. H. MacDonald, B. A. Bernevig, A. Yazdani, *Science* **2014**, *346*, 602.
[23] H. Weng, X. Dai, Z. Fang, *Phys. Rev. X* **2014**, *4*, 011002.
[24] C. Felser, E. W. Finckh, H. Kleinke, *J. Mater. Chem.* **1998**, *8*, 1787.
[25] M. W. Oh, B. S. Kim, S. D. Park, W. D. Mee, H. W. Lee, *Solid State Commun.* **2008**, *146*, 454.
[26] S. Furuseth, L. Brattas, A. Kjekshus, *Acta Chem. Scand.* **1973**, *27*, 2367.
[27] S. Saibene, T. Butz, A. Lerf, F. Levy, W. Abriel, *Hyperfine Interact.* **1990**, *60*, 907.
[28] F. Nichele, H. J. Suominen, M. Kjaergaard, C. M. Marcus, E. Sajadi, J. A. Folk, B.-M. Nguyen, A. A. Kiselev, W. Yi, M. Sokolich, M. J. Manfra, E. M. Spanton, K. A. Moler, **2015**, DOI: arxiv.org/abs/1511.01728.
[29] L. Brattas, A. Kjekshus, *Acta Chem. Scand.* **1972**, *26*, 3441.
[30] J. Bardeen, L. N. Cooper, J. R. Schrieffer, *Phys. Rev. Lett.* **1957**, *108*, 1175.
[31] C. Nayak, S. H. Simon, A. Stern, M. Freedman, S. Das Sarma, *Rev. Mod. Phys.* **2008**, *80*, 1083.
[32] A. Y. Kitaev, *Ann. Phys.* **2003**, *303*, 2.